PROCEEDINGS OF SCIENCE

COUPLING THE DYNAMICS OF STATISTICALLY DISTRIBUTED AND EXCESS DISLOCATIONS

Satya VARADHAN
Department of Mechanical and Industrial Engineering
University of Illinois at Urbana - Champaign
1206 West Green Street, Urbana, IL 61801, USA
E-mail: varadhan@uiuc.edu

Armand J. BEAUDOIN
Department of Mechanical and Industrial Engineering
University of Illinois at Urbana - Champaign
1206 West Green Street, Urbana, IL 61801, USA
E-mail: abeaudoi@uiuc.edu

Claude FRESSENGEAS*
Laboratoire de Physique et Mécanique des Matériaux
Université de Metz / CNRS
Ile du Saulcy, 57045 Metz Cedex, France
E-mail: claude.fressengeas@univ-metz.fr

Modeling the self-organization and collective behavior of dislocation ensembles is of primary concern in this work. Two dislocation species are considered: excess dislocations seen as a manifestation of lattice incompatibility, and statistically distributed dislocations, which induce compatible deformation. Conventional slip-based crystal plasticity is used to model the behavior and dynamics of the latter, while Field Dislocation Mechanics is employed to account for the former. Coupling the dynamics of both species proceeds along two reciprocal ways: spatial gradients in slip produced by mobile statistical dislocations leads to nucleation of excess dislocations, while excess dislocations contribute to forest hardening. Illustration is given to the evolution of mobile and excess dislocation density. Dislocation arrangements resulting from the model are presented.

International Conference on Statistical Mechanics of Plasticity and Related Instabilities
31 August - 2 September 2005
Bangalore, India

*Speaker.

PoS(SMPRI2005)004

1. Introduction

In conventional theories of continuum crystal plasticity, the state variables are plastic strain rate and stress. Dislocations - the underlying defects at the origin of plasticity - are usually overlooked in the description, a valid point of view as long as their spatial distribution is uncorrelated. Such an assumption loses validity when dislocation interactions become strong enough, which occurs sooner or later in the course of plastic deformation. Then, self-organization of dislocation ensembles and collective behavior involving large numbers of correlated events occur at intermediate length scales. Prominent examples of such behavior are persistent slip bands in fatigue, Lüders and Portevin - Le Chatelier bands, all characterized by strongly non-uniform spatial distributions of dislocation ensembles.

Building a tractable link between these non-uniform distributions and macroscopic observable manifestations of plasticity is currently a challenge addressed to the mechanical/material community. A recent advance in this respect has been to account for "excess dislocations" (EDs) as a manifestation of lattice incompatibility, as opposed to "statistically distributed dislocations" (SDs), which result in compatible deformation. These two concepts are scale-dependent, and at a sufficiently fine scale of spatial resolution, all dislocations are EDs. Acharya recently developed a continuum framework, Field Dislocation Mechanics (FDM), well suited to the fine scale of resolution, with dislocation density and stress as state variables [1]. FDM provides for the dynamic evolution of EDs and stress fields as the solution of a boundary value problem. In practice it is applicable to systems with sufficiently small dimensions. At larger scales of resolution, EDs offset each other and SDs are inevitably present. As both EDs and SDs contribute to plastic deformation, building a combined model for the dynamic evolution of both EDs and SDs thus becomes desirable. A framework for such combined models has been set forth in [2], [3].

In this presentation, slip-based conventional crystal plasticity is used to model the behavior of SDs, while FDM is used for ED dynamics. Coupling the compatible and incompatible parts of dislocation dynamics is achieved in two reciprocal ways: differential slip of SDs leads to ED nucleation, while EDs contribute to forest hardening. Evolution equations for the statistical dislocation densities round out the proposed model. The paper is organized as follows. Section 2 is devoted to a presentation of small strain Field Dislocation Mechanics. In Section 3, a model is outlined, which combines conventional crystal plasticity with FDM. Application of this combined model to the yield point phenomenon is shown in Section 4. Final remarks and an overall discussion are provided in Section 5.

2. Field dislocation Mechanics

Dislocations have an interaction stress field, which results from their non homogeneous spatial distribution. In combination with the stress field due to the applied traction and displacement boundary conditions, this stress field contributes to driving the motion of dislocations, which results in permanent deformation of the crystalline solid. The aim of FDM is to provide a continuum description of this coupled process by using the mathematical framework of partial differential equations. As

a result of the theory, the dynamic evolution of the dislocations and stress fields should emerge as the solution of a boundary value problem.

Let us consider a crystalline domain D, subject to usual traction and displacement boundary conditions on its outer surfaces ∂D_t and ∂D_u. At small strains, the distortion (or displacement gradient) $\mathbf{U} = \text{grad}\ \mathbf{u}$ can be additively split into its elastic and plastic part, $\mathbf{U}_e$ and $\mathbf{U}_p$ respectively. In turn, each part can be split into its compatible $(\mathbf{U}_e^{\parallel}, \mathbf{U}_p^{\parallel})$ and incompatible $(\mathbf{U}_e^{\perp}, \mathbf{U}_p^{\perp})$ components, with the combinations

$$\text{grad}\ \mathbf{u} = \mathbf{U}_e^{\parallel} + \mathbf{U}_p^{\parallel}, \quad \mathbf{U}_e^{\perp} + \mathbf{U}_p^{\perp} = 0 \tag{2.1}$$

The continuum description of dislocations needed by FDM is based upon Nye's dislocation density tensor $\boldsymbol{\alpha}$ [4]. Operating on the normal $\mathbf{n}$ to a unit surface S, $\boldsymbol{\alpha}$ provides the net Burgers vector $\mathbf{b} = \boldsymbol{\alpha} \cdot \mathbf{n}$ of all dislocations lines threading S, i.e., the closure failure of the Burgers circuit surrounding this surface. Using Nye's tensor, which incorporates information on dislocation line direction, is essential to the determination of the incompatible distortion tensors $(\mathbf{U}_e{}^{\perp}, \mathbf{U}_p{}^{\perp})$ through equations

$$\text{curl}\ \mathbf{U}_e^{\perp} = -\text{curl}\ \mathbf{U}_p^{\perp} = \boldsymbol{\alpha} \tag{2.2}$$

The solution to these equations is known up to a gradient. In order ensure that no component belonging to the null-space of the curl operator is involved in the solution, the additional equation $\text{div}\ \mathbf{U}_e^{\perp} = 0$ and boundary condition $\mathbf{U}_e^{\perp} \cdot n = 0$ on ∂D are imposed (say on $\mathbf{U}_e^{\perp}$). In FDM, $\dot{\mathbf{U}}_p^{\parallel}$ is constitutively specified as the null-space (compatible) component of the slip plastic distortion rate $\dot{\mathbf{U}}_p$

$$\dot{\mathbf{U}}_p = \boldsymbol{\alpha} \times \mathbf{v} + \mathbf{L}_p \tag{2.3}$$

Throughout this paper, a dot denotes the time derivative. $\mathbf{v}$ stands for the velocity of dislocations, which will be provided constitutively later on (see Eqs. 2.7, 2.8, 3.5) in terms of stresses and dislocation densities. $\mathbf{L}_p$ is a velocity gradient, taken to be identically zero in this Section. Unless stated otherwise, the following statements are valid for a non zero $\mathbf{L}_p$. The interpretation for $\mathbf{L}_p$ will be given in the next Section. In the absence of $\mathbf{L}_p$, the relation 2.3 between distortion slip rate, dislocation density and velocity, has the interpretation of being a tensorial Orowan relation. The tensor $(\boldsymbol{\alpha} \times \mathbf{v}) \cdot d\mathbf{x}$ is the flux of Burgers vectors across a curve element $d\mathbf{x}$. Selected by the curl operator, the incompatible part of $\dot{\mathbf{U}}_p$ feeds the increment of excess dislocations through the equation of balance for closure defects

$$\dot{\boldsymbol{\alpha}} = -\text{curl}\ \dot{\mathbf{U}}_p \tag{2.4}$$

Equation 2.4 expresses the conservation of closure failure in a Burgers circuit attached to the deforming crystal. It can also be seen as the evolution equation for the dislocation density α. The stress field $\mathbf{T}$ is written in terms of the elastic or plastic distortions as

$$\mathbf{T} = \mathsf{C}^e : \{\mathbf{U}_e^{\parallel} + \mathbf{U}_e^{\perp}\} = \mathsf{C}^e : \{\text{grad}\ \mathbf{u} - \mathbf{U}_p^{\parallel} - \mathbf{U}_p^{\perp}\} \tag{2.5}$$

where C^e is the elastic constitutive tensor and $\{\mathbf{A}\}$ denotes the symmetric part of tensor $\mathbf{A}$. The stress tensor $\mathbf{T}$ satisfies the equilibrium equation

$$\operatorname{div} \mathbf{T} = 0 \tag{2.6}$$

Based on thermodynamic guidelines resulting from the Clausius-Duhem inequality (the dissipation should be non–negative), the dislocation velocity is taken to be of the form

$$\mathbf{v} = \bar{v}\frac{\xi}{|\xi|} \tag{2.7}$$

$$\xi = \mathbf{X}(\mathbf{T} : \boldsymbol{\alpha}) \tag{2.8}$$

where $\bar{v}$ specifies its magnitude (see below Eq. 3.5) and $\mathbf{X}$ represents the permutation tensor. Eq. 2.8 prescribes the direction ξ of the dislocation velocity. The latter is found to be normal to the dislocation line, as expected from common knowledge. Suitable boundary conditions are imposed to ensure closure of the theory. In particular, no inward flux of dislocations across external surfaces is allowed, whereas outflow of dislocations is unrestricted.

As such, FDM is a closed theory in the sense that it has enough statements to uniquely determine the stress and dislocation fields. In principle, it can be applied to material systems at any scale. In practice, due to limited computational resources, it only applies to micro-systems. However, increasing the size of the Burgers circuits used to express incompatibility allows to deal with larger systems, while smearing out the smallest details of dislocation distributions. This process is further detailed in the next Section.

3. Combined model

The distortion rate $\mathbf{L_p}$ introduced above in Eq. 2.3 is now non zero. It is assumed to originate in the motion of statistical dislocations, as is usual in conventional crystal plasticity. Through this term, generation of excess dislocations is obtained from the non uniformity of the conventional distortion rate field. Other sources of excess dislocation generation, such as line length increase, are included in the flux term $\boldsymbol{\alpha} \times \mathbf{v}$ of the distortion rate $\dot{\mathbf{U}}_p$ [5]. Let the Schmid orientation tensor of slip system s be

$$\mathbf{P}_s = \mathbf{b}_s \otimes \mathbf{n}_s \tag{3.1}$$

where $\mathbf{b_s}$ denotes the slip direction and $\mathbf{n_s}$ is the unit normal to the slip plane. Combining all slip systems, the distortion rate tensor is

$$\mathbf{L}_p = \sum_s \rho_m b v_s \mathbf{P}_s \tag{3.2}$$

Here ρ_m is a mobile statistical dislocation density, in units of dislocation line length per volume, b is the Burgers vector modulus and v_s a dislocation velocity. For simplicity, only one mobile dislocation density common to all slip systems, is considered here. The total equivalent strain rate from both ED and SD activity is

$$\dot{\Gamma} = |\dot{\mathbf{U}}_p| \tag{3.3}$$

where the symbol $|\mathbf{a}|$ stands for the norm of $\mathbf{a}$. The velocity v_s is known from the resolved shear stress $\tau_s = \mathbf{T} : \mathbf{P_s}$, taken in this work as a power law

$$v_s = v_0 \mathrm{sgn}(\tau_s) \left| \frac{\tau_s}{\tau_0 + \tau_h} \right|^m \tag{3.4}$$

Here v_0 is a reference velocity and τ_0 is an athermal contribution to the slip system obstacle strength. The stress exponent m is taken as 20 in this work, providing a response that is relatively insensitive to strain rate. The magnitude $\bar{v}$ of the velocity of EDs (see Eq. 2.7) follows a similar relationship

$$\bar{v} = v_0 \mathrm{sgn}(\tau) \left| \frac{\tau}{\tau_0 + \tau_h} \right|^m \tag{3.5}$$

$$\tau = \frac{\boldsymbol{\alpha} \times \mathbf{v}}{|\boldsymbol{\alpha} \times \mathbf{v}|} : \mathbf{T} \tag{3.6}$$

The stress τ_h is needed to overcome forest obstacles to dislocation motion. According to the Bailey-Hirsch formulation, it is taken as

$$\tau_h = \tilde{\alpha} \mu b \sqrt{\rho_f} \tag{3.7}$$

$\tilde{\alpha}$ is a constant, μ the shear modulus, and ρ_f stands for the statistical forest dislocation density. In this work, the time evolution of both ρ_m and ρ_f is obtained from the Kubin - Estrin model [6]

$$\dot{\rho}_m = ((C_1/b^2) - C_2 \rho_m - (C_3/b)\sqrt{\rho_f})\dot{\Gamma} \tag{3.8}$$

$$\dot{\rho}_f = (C_0 b|\alpha| + C_2 \rho_m + (C_3/b)\sqrt{\rho_f} - C_4 \rho_f)\dot{\Gamma} \tag{3.9}$$

In these equations, C_1 accounts for mobile dislocation multiplication, C_2 is for mutual annihilation and concomitant debris generation, C_3 stands for immobilization on forest obstacles and C_4 for dynamic recovery. We introduce in addition the term C_0, meant to account for the contribution of EDs to forest hardening [7]. Together with Eqs. 2.3, this term provides for the coupling between ED and SD dynamics through work hardening. In the absence of EDs, obtained by setting $\boldsymbol{\alpha} = 0$ in the above equations, the present model reduces to a conventional crystal plasticity formulation. In the absence of the distortion rate $\mathbf{L_p}$, it reduces to FDM.

4. Numerical formulation and results

The equations for the combined model set forth in Section 3 form a coupled set of partial differential equations, which can be solved numerically by using a finite element scheme. A brief outline of the algorithm we employed is provided in the following. A more detailed account can be found in Ref. [8]. At time t, known dislocations densities lead to solving Eq. 2.2 for the incompatible plastic distortion. In combination with the compatible part of Eq. 2.3, this solution leads to the

b	τ_a	v_0	$\rho_m(0)$	$\rho_f(0)$
0.27 [nm]	6.54 [MPa]	3.75×10^{-8} [m/s]	10^{12} [m^{-2}]	10^{11} [m^{-2}]
C_0	C_1	C_2	C_3	C_4
20.0	2.43×10^{-5}	3.03	8.18×10^{-3}	3.33

Table 1: Parameters used in the simulations.

plastic distortion. The equilibrium equation 2.6 is then used to solve for the displacement $\mathbf{u}$. The rearrangement of the dislocations resulting from the stress field is obtained at time $t+\Delta t$ from the evolution equation 2.4. Finally, the slip plastic distortion is evolved to time $t+\Delta t$ by using the rate equation 2.3. Input from crystal plasticity at time t is taken in solving the equilibrium equation and in this update.

Central to the design of the combined model is the production of ED sources through gradients in the plastic deformation from crystal plasticity. In the numerical implementation, the distortion rate $\mathbf{L}_p$ from time t enters into Eq. 2.3 for evaluation at the subsequent time step $t+\Delta t$. Integration of Eq. 2.3 by parts reveals the formulation presented herein as one specific choice of possible boundary conditions outlined in [2], with $\mathbf{L}_p \times \mathbf{n}$ specified on the entire boundary. In addition, we specify $\boldsymbol{\alpha}(\mathbf{v}\cdot\mathbf{n}) = \mathbf{0}$ on the inflow boundary, as indicated above.

Standard Galerkin formulations are known to be unstable for first-order hyperbolic equations such as the transport equation 2.4. Thus, a mixed Galerkin-Least-Squares finite element method is introduced for 2.4 [5], while a Least-Squares formulation is used to solve for the incompatibility equation 2.2. A standard Galerkin scheme is used for the rest of the equations. The integration uses an explicit Euler scheme.

Illustration of the above developments is sought in the investigation of the yield point phenomenon in simple tension of an idealized crystal with dimensions 1.5 [μm] $\times$ 1.5 [μm] $\times$ 3.0 [μm]. Four different simulations were undertaken in order to illustrate features of the solutions following from FDM, conventional crystal plasticity and the combined model.

- Using FDM, a single slip system with $\mathbf{n} = \left[-\frac{1}{\sqrt{2}} \;\; 0 \;\; \frac{1}{\sqrt{2}}\right]^T$ and $\mathbf{b} = \left[\frac{1}{\sqrt{2}} \;\; 0 \;\; \frac{1}{\sqrt{2}}\right]^T$ is initialized with a constant mobile edge density. Two simulations were performed with initial densities of magnitude 10 [m^{-1}] and 100 [m^{-1}]. The specification of a spatially constant density leads to a state of zero initial stress. A mesh of $12 \times 12 \times 24$ elements is employed and kinematic boundary conditions are prescribed representing a uniaxial tension.

- In a third simulation using only crystal plasticity, the usual FCC slip systems are taken with a cube orientation. This leads to symmetric slip and a constant $\mathbf{L}_p$. The mesh and boundary conditions are taken as for the FDM case, above.

- Finally, we exercise the combined model by specifying the twelve (statistical) slip systems such that a 'primary' slip plane is coincident with the same FDM plane given above. A more

refined mesh is taken, consisting of $24 \times 24 \times 48$ elements. Additional displacement degrees of freedom are constrained in the combined model simulation which promote a non-uniform deformation, to be described.

Young's modulus and Poisson's ratio were taken as 70 GPa and 0.3, respectively. Other material parameters are given in Table 1.

The stress strain response is plotted in figure 1. An applied strain rate of $10^{-3}\ s^{-1}$ is used in all simualtions. The elasto-viscoplastic transition is predicted by conventional crystal plasticity and the combined model. The apparent difference in the modulus for the combined model result is due to the fact that this nominal stress is drawn from a non-uniform deformation. The stress strain response obtained from FDM with lower initial density displays an apparently elastic response. With increased density, an initial elastic increase is followed by a limited amount of plasticity through Eq. 2.3, eventually ending in an exotic elastic increase. This behavior has its origin in the exhaustion of the initial dislocation densities in the absence of a source term, which flow out of the crystal through its external boundaries. This is shown in figure 2. The mobile edge density flows along the prescribed slip plane and out of the crystal, providing only a very small plastic strain commensurate with the initial density. Along with the boundary condition for zero inflow, $\boldsymbol{\alpha}(\mathbf{v}\cdot\mathbf{n}) = \mathbf{0}$ this leads to an essentially defect-free (source starved) crystal.

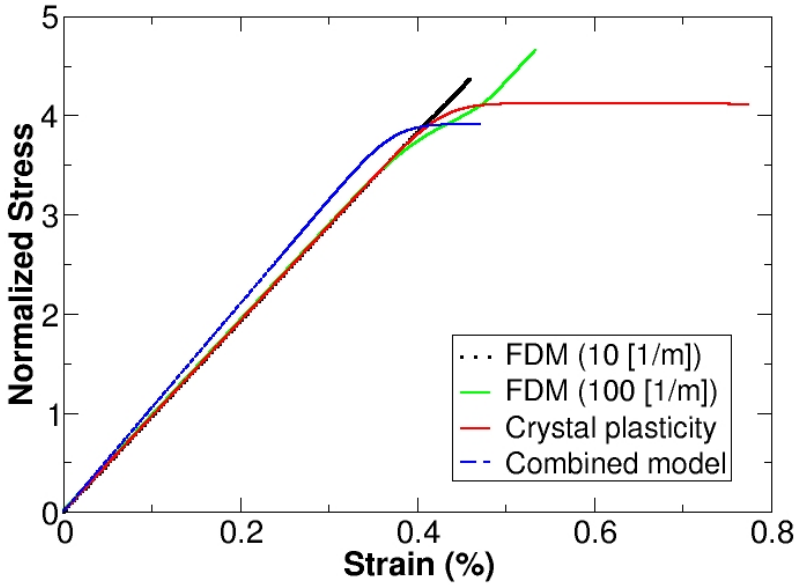

Figure 1: Stress strain response for the simulations, normalized by $\tau_0 + \tau_h(0)$.

The behavior of the combined model is much more complex. The mobile components and magnitude of the ED are shown in figure 3, corresponding to the end point of the stress–strain curve of figure 1. The initial ED was specified as zero in this simulation, however, displacement

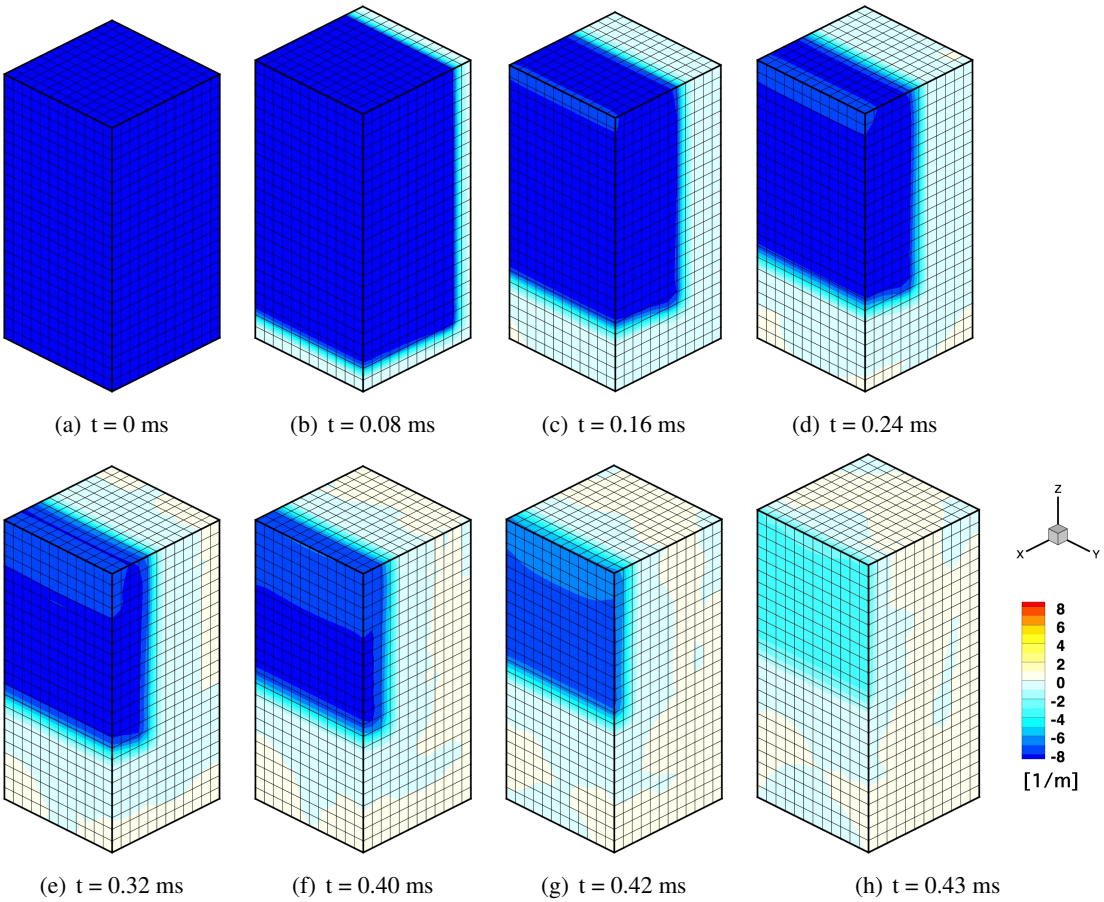

(a) t = 0 ms (b) t = 0.08 ms (c) t = 0.16 ms (d) t = 0.24 ms

(e) t = 0.32 ms (f) t = 0.40 ms (g) t = 0.42 ms (h) t = 0.43 ms

Figure 2: Transport of initial edge density of 10m^{-1} using FDM.

components in the x and y directions were constrained on the top and bottom faces. [This is in addition to the presciption of a zero and fixed vertical displacement rate on the bottom and top surfaces, respectively, as was done in the other simulations.] Such constraint leads to a spatially varying distortion $\mathbf{L}_p$, setting off source evolution in the combined model through Eq. 2.3. The slices shown in figure 3a reveal the mobile components of the ED with a pure screw and edge character, on planes with normal in the x and y directions, respectively. The pattern of the edge density *magnitude* is rotationally symmetric about the y axis (somewhat obstructed by the plane showing screw density. For both screw and edge components, the opposing sign of the ED is observed on each side of the centerline. This gives the impression of a loop structure. Figure 3b reveals the magnitude of the ED. Low density is observable adjacent to the constrained ends of the specimen. Deformation tending towards uniaxial tension is expected at the specimen center, and here the ED appears lessened. Highest density is present proximal to the ends of the specimen, where gradients in $\mathbf{L}_p$ are expected.

5. Final remarks and conclusion

In the presence of patterning at some intermediate scale in the materials microstructure, non local

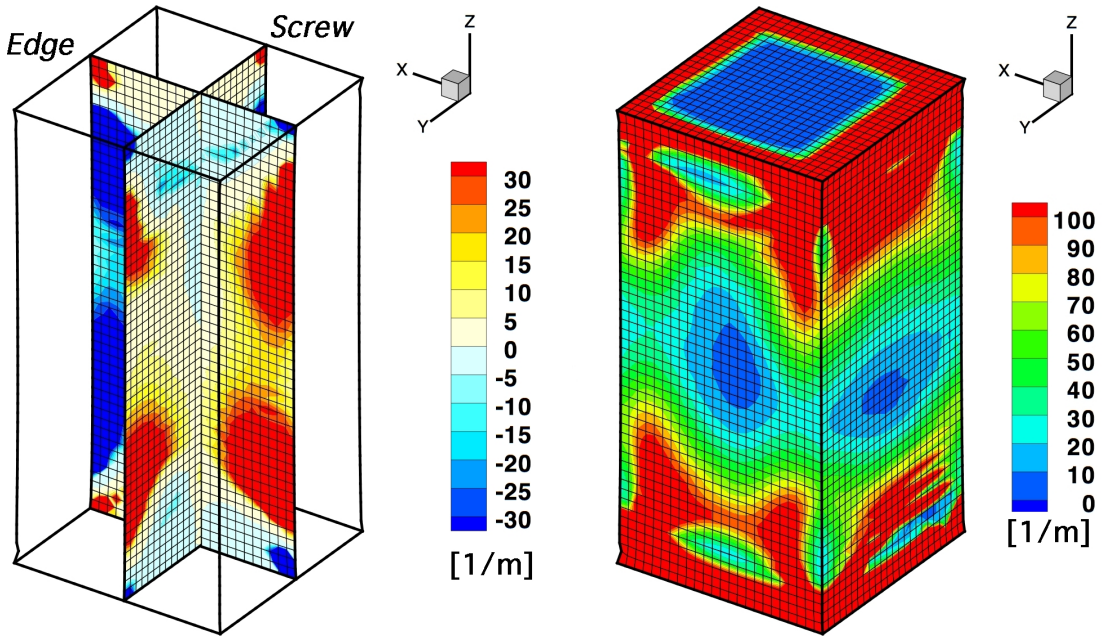

(a) Mobile components in slip plane. (b) $|\boldsymbol{\alpha}|$ of the excess dislocation density tensor.

Figure 3: Excess dislocation density

dynamic theories of plasticity are needed. Local models such as conventional crystal plasticity do not involve a characteristic length scale, and they are therefore unable to account for such patterning phenomena. Introducing in a phenomenological way these length scales in the constitutive equations for plasticity, by accounting for gradients of strain or rotation, has been shown to offer a workable alternative in the characterization of the emerging patterns (see for example [9], [10]). However, the identification of the involved length scales and their physical justification remains mostly a matter of controversy.

Lattice incompatibility is inherent to plasticity, and is known to provide for the spatial interactions that are central to non local models, through the internal elastic stresses that it generates [11], [12]. Dislocation transport has also been formalized in the last decades [13], and may be taken as an undisputable source for spatial coupling because of its geometric foundation. However, it has been realized only recently that lattice incompatibility and dislocation transport could be combined to build dynamic field equations for dislocation densities and stresses [1]. The resulting model, FDM, is a theory of plasticity which naturally incorporates physically-based length scales and spatial interactions due to dislocation activity.

The present theory builds on the basic equations of FDM. It additionally provides a source for lattice incompatibility in the non uniformities of conventional crystal plasticity. Besides, excess dislocations enter the description of forest hardening due to statistical dislocations, thus offering a two-ways dynamic coupling between the two dislocation species. Consequently, the present model has the potential to offer a dynamic description of dislocation patterning at an intermediate length

scale. It contains both FDM and crystal plasticity as limiting cases at very small or very large scales of resolution respectively. The classical (and powerful) framework of boundary value problems and partial differential equations is conservatively employed. The model is therefore amenable to (more or less) conventional weak forms and finite element schemes. Finite deformations and the large dislocation densities they entail are not expected to raise practically or conceptually unsolvable problems. Extensions of the model to such situations can be forecasted in the near future [3]. We believe, on the basis of the above results, that the present model could be a useful tool in dealing with such problems as strain hardening, pattern formation and instabilities at the mesoscale, or back-stress concepts and complex deformation paths.

6. Acknowledgments

We are indebted to Prof. Amit Acharya of Carnegie Mellon University for ongoing and thoughtful discussion, as well as comments on this manuscript. AB and SV received support under the US Department of Energy Stewardship Science Academic Alliances Program (DOE DEFG03-02-NA00072) and Center for Simulation of Advanced Rockets at the University of Illinois at Urbana-Champaign (US DOE subcontract B341494). The co-authors benefited from exchanges under a joint agreement between Centre National de la Recherche Scientifique and the University of Illinois at Urbana-Champaign. We are thankful for the invitation and happy to have participated in this conference in honor of Prof. G. Ananthakrishna.

References

[1] A. Acharya, *A model of crystal plasticity based on the theory of continuously distributed dislocations*, J. Mech. Phys. Solids, **49**, 761, 2001.

[2] A. Acharya and A. Roy, *Size effects and idealized dislocation microstructure at small scales: Predictions of a phenomenological model of mesoscopic field dislocation mechanics: Part I*, accepted for publication in J. Mech. Phys. Solids.

[3] A. Acharya and A. Roy, *Size effects and idealized dislocation microstructure at small scales: Predictions of a phenomenological model of mesoscopic field dislocation mechanics: Part II*, accepted for publication in J. Mech. Phys. Solids.

[4] J.F. Nye, *Some geometrical relations in dislocated crystals*, Acta Metall., **1**, 153, 1953.

[5] S. Varadhan, A.J. Beaudoin, A. Acharya and C. Fressengeas, *Dislocation transport using an explicit Galerkin/Least-Squares formulation*, submitted.

[6] L.P. Kubin and Y. Estrin, *Evolution of dislocation densities and the critical conditions for the* P*ortevin*-L*e* C*hatelier effect*, Acta Metall. Mater., **38**, 697, 1990.

[7] A. Acharya and A. J. Beaudoin, *Grain-size effect in viscoplastic polycrystals at moderate strains*, J. Mech. Phys. Solids., **48**, 2213, 2000.

[8] A. Roy and A. Acharya, *Finite element approximation of field dislocation mechanics*, J. Mech. Phys. Solids **53** 143, 2005.

[9] E.C. Aifantis, Mat. Sci. and Eng., *On the dynamical origin of dislocation patterns*, **81**, 563, 1986.

[10] N.A. Fleck, G.M. Muller, M.F. Ashby and J.W. Hutchinson, *Strain gradient plasticity: theory and experiment*, Acta Metall Mater, **42**,475, 1994.

[11] E. Kröner and A. Seeger, *Nicht-lineare Elastizitätstheorie der Versetzungen und Eigenspannungen*, Arch. Rat. Mech., **3**, 97, 1959.

[12] J.R. Willis, *Second-order effects of dislocations in anisotropic crystals*, Int. J. Engng. Sci., **5**, 171, 1967.

[13] T. Mura, *Continuous distribution of moving dislocations*, Phil. Mag., **89**, 843, 1963.